AFRL-RX-WP-TP-2008-4312

VARIABILITY IN ROOM TEMPERATURE FATIGUE LIFE OF ALPHA+BETA PROCESSED Ti-6Al-4V (PREPRINT)

Patrick J. Golden, Reji John, and John Porter

Metals Branch
Metals, Ceramics, and NDE Division

OCTOBER 2008

AIR FORCE RESEARCH LABORATORY
MATERIALS AND MANUFACTURING DIRECTORATE
WRIGHT-PATTERSON AIR FORCE BASE, OH 45433-7750
AIR FORCE MATERIEL COMMAND
UNITED STATES AIR FORCE

REPORT DOCUMENTATION PAGE

Form Approved
OMB No. 0704-0188

1. REPORT DATE *(DD-MM-YY)*	2. REPORT TYPE	3. DATES COVERED *(From - To)*
October 2008	Journal Article Preprint	

4. TITLE AND SUBTITLE
VARIABILITY IN ROOM TEMPERATURE FATIGUE LIFE OF ALPHA+BETA PROCESSED Ti-6Al-4V (PREPRINT)

5a. CONTRACT NUMBER
In-house

5b. GRANT NUMBER

5c. PROGRAM ELEMENT NUMBER
62102F

6. AUTHOR(S)
Patrick J. Golden and Reji John (AFRL/RXLMN)
John Porter (University of Dayton Research Institute)

5d. PROJECT NUMBER
4347

5e. TASK NUMBER
RG

5f. WORK UNIT NUMBER
M02R3000

7. PERFORMING ORGANIZATION NAME(S) AND ADDRESS(ES)
Metals Branch (AFRL/RXLMN)
Metals, Ceramics, and NDE Division
Materials and Manufacturing Directorate
Wright-Patterson Air Force Base, OH 45433-7750
Air Force Materiel Command, United States Air Force

University of Dayton Research Institute

8. PERFORMING ORGANIZATION REPORT NUMBER
AFRL-RX-WP-TP-2008-4312

9. SPONSORING/MONITORING AGENCY NAME(S) AND ADDRESS(ES)
Air Force Research Laboratory
Materials and Manufacturing Directorate
Wright-Patterson Air Force Base, OH 45433-7750
Air Force Materiel Command
United States Air Force

10. SPONSORING/MONITORING AGENCY ACRONYM(S)
AFRL/RXLMN

11. SPONSORING/MONITORING AGENCY REPORT NUMBER(S)
AFRL-RX-WP-TP-2008-4312

12. DISTRIBUTION/AVAILABILITY STATEMENT
Approved for public release; distribution unlimited.

13. SUPPLEMENTARY NOTES
Journal article submitted to *International Journal of Fatigue*.

PAO Case Number: 88ABW 2008-0371; Clearance Date: 02 Oct 2008. The U.S. Government is joint author of this work and has the right to use, modify, reproduce, release, perform, display, or disclose the work.

14. ABSTRACT
In this program, smooth bar fatigue tests were conducted by several laboratories on the same lot of Ti-6Al-4V forged plate material. Multiple stress ratios and stress levels were tested to generate a fully populated stress-life curve. The tests, however, did not typically consist of many repeats. The approach of this work is to conduct a statistically significant number of repeated fatigue tests at a few loading conditions. A similar approach has been performed on several other turbine engine material systems often revealing a bimodal life distribution consisting of a number of low life specimens that may fail due to a separate mechanism. This paper will discuss the Ti-6Al-4V life distributions and sources of variability. Crack propagation using small crack growth data is used to predict the low life failures. Methods of modeling and predicting the life distributions will be discussed and demonstrated.

15. SUBJECT TERMS
fatigue nucleation, fatigue crack growth, life variability, Ti-6Al-4V, small crack growth

16. SECURITY CLASSIFICATION OF:			17. LIMITATION OF ABSTRACT:	18. NUMBER OF PAGES	19a. NAME OF RESPONSIBLE PERSON (Monitor)
a. REPORT	b. ABSTRACT	c. THIS PAGE			James M. Larsen
Unclassified	Unclassified	Unclassified	SAR	22	19b. TELEPHONE NUMBER *(Include Area Code)* N/A

Variability in Room Temperature Fatigue Life of Alpha+Beta Processed Ti-6Al-4V

Patrick J. Golden [a,*], Reji John [a], John Porter [b]

[a] US Air Force Research Laboratory, AFRL/RXLMN, Wright-Patterson AFB, OH 45433, USA
[b] University of Dayton Research Institute, Dayton, OH 45469, USA

Abstract

In this program, smooth bar fatigue tests were conducted by several laboratories on the same lot of Ti-6Al-4V forged plate material. Multiple stress ratios and stress levels were tested to generate a fully populated stress-life curve. The tests, however, did not typically consist of many repeats. The approach of this work is to conduct a statistically significant number of repeated fatigue tests at a few loading conditions. A similar approach has been performed on several other turbine engine material systems often revealing a bimodal life distribution consisting of a number of low life specimens that may fail due to a separate mechanism. This paper will discuss the Ti-6Al-4V life distributions and sources of variability. Crack propagation using small crack growth data is used to predict the low life failures. Methods of modeling and predicting the life distributions will be discussed and demonstrated.

Keywords

Fatigue Nucleation, Fatigue Crack Growth, Life Variability, Ti-6Al-4V, Small Crack Growth

1. Introduction

The current life management approach for maintaining most of the aerospace components in the U.S. Air Force is based on two specifications known as the Engine Structural Integrity Program (ENSIP) [1] and the Aircraft Structural Integrity Program (ASIP) [2]. These specifications, which are based on traditional views of statistical behavior of materials, are often very conservative, resulting in significant sustainment costs. Hence, the Air Force is pursuing the prognosis approach [3], which is based on the development and integration of new capabilities for real-time state awareness, physics-based damage and failure modeling, and autonomic reasoning. Reliable prognosis of a component depends on basic understanding and modeling of the sources of uncertainty in material behavior under service loading conditions. Physics-based probabilistic material models are, therefore, essential for accurately predicting fatigue life and the associated uncertainty. Since these models are based on observed damage mechanisms, prediction of the design fatigue life limit, e.g. 1 in 1000 probability of failure, can be expected to be more accurate than statistical estimations based on data. Recent examples of physics-based probabilistic fatigue life prediction models include approaches proposed by Magnusen et al. [4], Chan et al. [5], Tryon et al. [6], Laz et al. [7], and Jha et al. [8-9]. Based on extensive characterization of the fatigue behavior, Jha et al. [8-9] also showed that the fatigue life distribution on a cumulative distribution function (CDF) plot exhibited a dual failure mode (bi-modal distribution) at some stress levels, i.e. a single CDF could not describe all the data. Limited [10] fatigue data available for alpha+beta processed Ti-6Al-4V does not exhibit the dual mode CDF observed by Jha et al. [8-9]. In addition, the effectiveness of the probabilistic fatigue life models for Ti-6Al-4V [5,6] to accurately capture the limiting life (lower end of the range of

* Corresponding author: Tel.: +1-937-255-5438; fax: +1-937-656-4840. E-mail address: patrick.golden@wpafb.af.mil

life at a given loading condition) and actual trend in the CDF have not been demonstrated due to lack of significant data. Hence, a study was initiated to conduct a detailed investigation of variability in fatigue life of alpha+beta processed Ti-6Al-4V. This paper will discuss the observed fatigue lifetime variability, crack initiation and growth during these tests, effect of surface finish on the lifetime distribution and the application of a small-crack-growth-based model to predict the limiting fatigue life of Ti-6Al-4V.

2. Experimental Procedures

The material used in this study was Ti-6Al-4V from the United States Air Force High Cycle Fatigue (HCF) program [10]. The material was forged into plates. The material was $\alpha+\beta$ forged then solution treated and overaged at 932°C for 75 min, fan cooled, and mill annealed at 704°C for 2 h. The resulting microstructure was approximately 60% primary α and 40% transformed β. The elastic modulus was 116 GPa and the 0.2 % offset yield stress was 930 MPa. The ultimate tensile strength was 980 MPa. Cyclic-stress-strain curves were generated under the HCF program [10] from the results of multiple strain controlled low cycle fatigue (LCF) tests. The material was shown to cyclically soften and the cyclic yield stress was approximately 750 MPa.

Round bar fatigue specimens were machined from the Ti-6Al-4V forged plate as shown in Fig. 1. The gauge section diameter is 4.27 mm and the gauge length is 12.7 mm. The material was finished using low stress grinding (LSG) followed by longitudinal polish. LSG is specified such that a shallow compressive residual stress remains on the machined surface, and the final surface finish was specified as an R_a of 0.2 μm. The second surface finish was chosen to remove residual stresses and further improve surface roughness and eliminate scratches. The specimens were first stress-relief annealed (SRA) in vacuum at 704°C for 1 hour. Next, they were electropolished resulting in approximately 50 μm of material removal. The final surface finish had an Ra of approximately 0.05 μm. In the HCF program, the baseline fatigue test surface condition was LSG plus chemical milling to remove approximately 50 μm of material from the surface with the intent of removing surface residual stresses and marks due to machining. This chemical milling process was different from the electropolish process and this will need to be considered when comparing fatigue data in this study to prior work.

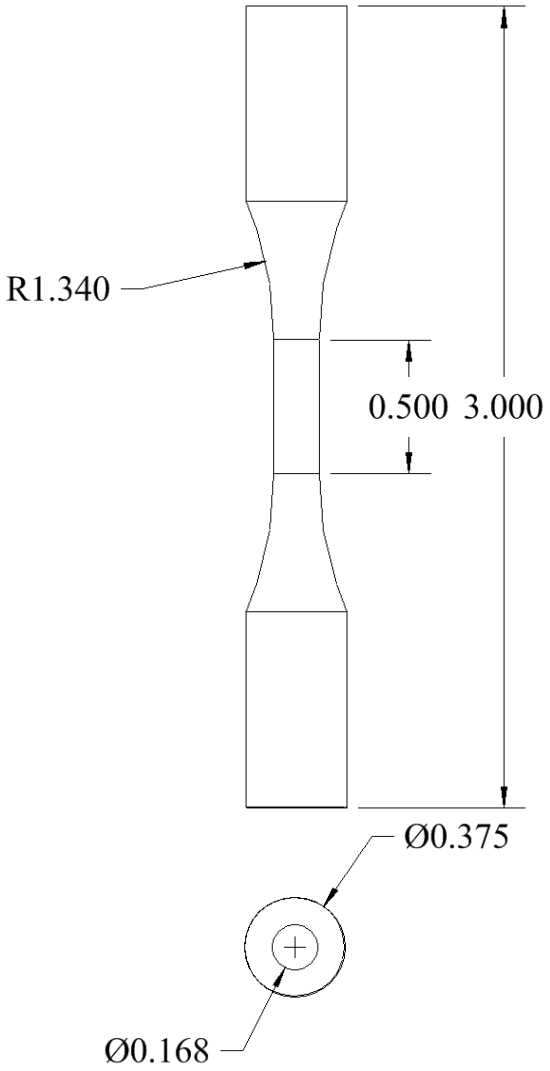

Figure 1: Drawing of the test specimen used in the project.

Testing was conducted on an MTS servo-hydraulic test machine. All testing was under constant amplitude load control with a stress ratio, *R*, of 0.1. The objective of this research was to determine the level of scatter in fatigue at several load conditions, therefore, stresses were chosen that would result in lives on the order of ten-thousand to ten-million cycles. Maximum stresses of 635 and 675 MPa were applied. Additionally, surface replicas were taken periodically on several of the specimens tested at both stresses. Four acetate tape replicas were taken at each increment of cycling; one on the front of the specimen, one on the back, and a repeat of each. The chosen increments of cycles were 5000 and 7500 cycles for 675 MPa and 635 MPa respectively at which time the test was stopped at a hold load of 60% of maximum. The replicas were taken blindly, that is they were not searched for cracks until after the specimen failed. At that time, the primary crack was easily found on the final set of replicas and tracked backwards on the earlier replicas.

3. Analytical Methods

The replica measurements were used to generate surface crack length, c, versus cycles, N, data so that the surface crack growth rate, dc/dN could be calculated. Here, c is half the total surface length of the crack. A 3 point sliding quadratic fit was used to smooth the c versus N data and to aid in the calculation of the derivative. A sliding quadratic fit using $n = 7$ points is common in crack growth test data reduction, however, this method of data reduction results in $n - 1$ fewer dc/dN points than the number of measurements. There are often very few replica crack measurements so $n = 3$ was chosen to minimize the amount of data lost during data reduction. The sliding quadratic fit used to calculate crack growth rates is further described in ASTM Standard E647 [11].

Analysis of the replica crack measurements collected from this research required some inference of the crack shape in the round bar. The crack shape was required in order to calculate the stress-intensity factor range, ΔK, to accompany the crack growth rate data, dc/dN. Two example crack shape assumptions are drawn in Fig. 2. Here, the dashed line represents the shape of a crack assumed in the numerical calculations of K made by Raju and Newman [12]. In this case the ratio of crack depth to half surface length, a/c, was equal to 1. Raju and Newman made no assumption about what the crack shape should be, but calculated K for cracks with $a/c = 0.6$, 0.8, and 1. The crack front was chosen to be elliptical in shape and the intersection of the crack front with the circular bar was constrained as perpendicular. The semi-major axis, semi-minor axis, and the center of the ellipse that formed this crack front were chosen to meet the crack size, shape, and intersection constraints given. The second crack shape drawn in Fig. 2 was take the work of Forman and Shivakumar [13]. This crack front shape was assumed circular and was also perpendicular to the surface of the round bar. This placed the center of the circle that formed the crack front outside the round bar and thus the radius of the crack front, r, was greater than the crack depth, a. This results in crack shape $a/c = 1$ as a/D approaches 0, and a/c decreases with increasing a/D to approximately $a/c = 0.7$ at $a/D = 0.4$. Here, D is the diameter of the round bar specimen. This assumption for crack shape was chosen by Forman because it appeared to be a lower bound conservative assumption. The data presented by Forman from the literature for Ti, however, showed that crack shapes for tension fatigue tests ranged from 0.92 to 1.0 regardless of crack depth.

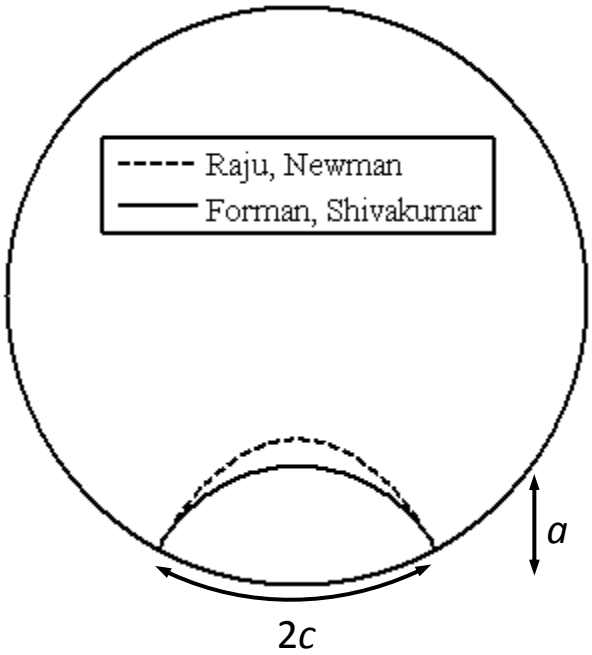

Figure 2: Drawing of two crack shape assumptions considered in the crack growth analysis [12,13].

The *K* analysis presented in this work was performed using the solutions published by Raju and Newman for *a*/*c* = 1.0 [12]. The primary emphasis of the fracture mechanics analysis was on short cracks with *a*/*D* close to zero in which case the crack shape assumptions of Forman and Shivakumar are also near *a*/*c* = 1. Short crack growth data from cracks measured using replicas were reduced using *a*/*c* = 1, and, likewise, all crack growth predictions were made assuming *a*/*c* = 1. Crack growth was calculated by integrating the d*a*/d*N* versus Δ*K* curve using the Euler method with a constant percent increment of crack growth for an assumed initial crack size and applied stress. The crack growth curve was fit from available data in the section below. The Raju and Newman *K* solutions had the form of Equations 1. Here *S* is the applied stress, *a* is the crack depth, *Q* is the square of the complete elliptic integral of the second kind and is a function of *a*/*c*, and *F* is the boundary correction factor and is a function of *a*/*D* and *a*/*c*. *F* was solved numerically using finite element analysis, but the solutions only extend down to *a*/*D* = 0.05. This was a concern since much of the crack growth in the specimens occurred at *a*/*D* < 0.05, therefore, the solutions for *F* were fit to a polynomial and extrapolated to *a*/*D* = 0.

$$K = S_i\sqrt{\pi\frac{a}{Q}}F \quad (1)$$

4. Results and Discussion

Repeat fatigue testing was conducted at R = 0.1 with 2 maximum stress levels (635 MPa and 675 MPa) and 2 surface conditions. The two surface conditions considered were LSG and stress-relief annealed (SRA) followed by electropolishing. Both conditions are described above. The results of in-depth residual stress measurements are plotted in Fig. 3. X-ray diffraction with a spot size of 1 mm was used to measure the residual stresses at several depths into the surface of the gauge section of the specimens. Layer removal was accomplished by electropolishing a

small region of the specimen. The residual stress results were corrected for stress gradient and layer removal effects [14]. The results show that the LSG surface had shallow compressive residual stresses, as expected, with a magnitude of 200-250 MPa at the surface. These stresses, however, quickly died out within 20 μm into the material. The residual stress on the SRA and electropolished samples appears to be nearly eliminated at the surface, however, it is slightly compressive (100 MPa) around 10 μm deep. The expected residual stress value at 30-80 μm into the material should be very near 0, however, all 3 measurements show approximately 40 MPa compressive residual stress. This has been a common observance in this Ti-6Al-4V material and it is hypothesized that this is a measurement phenomenon tied to the microstructure of the material. In any case, this small residual stress does not significantly influence the analysis or conclusions from this data.

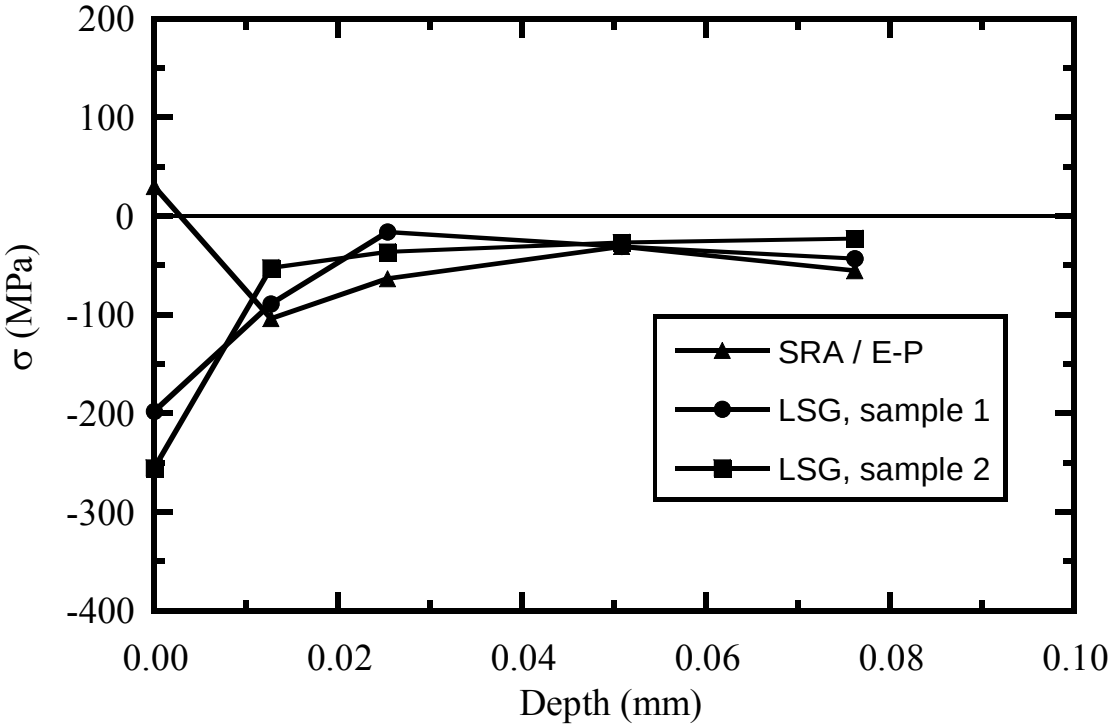

Figure 3: In-depth residual stress measurements in the axial direction of the specimens.

The test results from this study were plotted on a stress-life (S-N) diagram in Fig. 4. Also plotted were all of the HCF program S-N data at R = 0.1 with the baseline surface condition. Again, the surface condition in the HCF program was LSG plus chemical milling removal of 50 μm from the surface of the specimens. It appears that the mean and median behavior of the SRA and electropolish data from this study generally agrees with the HCF program data at both the 635 MPa and 675 MPa stress levels. There is a larger range of behavior in the 17 electropolished data at 675 MPa (65,000 to 554,000 cycles) than in the HCF program data near 675 MPa, however, this may simply be due to the much larger set of data in the current work. Only 3-4 tests per stress were conducted in the HCF program near that stress level which is not enough data to describe a statistical distribution of failures at that stress. It is impossible to know what range of behavior the HCF program data might have displayed with more testing. At 635 MPa the range in both the electropolished and HCF program data are fairly similar; however, this

doesn't necessarily signify that their distributions are the same. Unfortunately HCF program testing was not conducted at exactly 635 MPa, but testing at 620 and 655 MPa collectively had a smaller range in behavior. The standard deviation of the $\log_{10}(N_f)$ for the HCF program data was 0.40 and 0.34 log units for 620 and 655 MPa, respectively, while the standard deviation for the SRA and electropolished surface condition was a little higher at 0.45 log units. This could indicate that the electropolished surface condition results in more scatter, but a two sample statistical test for variance shows that this difference is not significant. The standard deviation of the $\log_{10}(N_f)$ at 675 MPa was 0.29 log units for electropolished data compared to 0.11 log units at 689 MPa in the HCF program data. Again, this difference is insignificant since there were only 3 tests in the HCF program data. The difference in the standard deviation of the electropolished data at 635 MPa (0.45 log units) and 675 MPa (0.29 log units) was found to be statistically significant with a p value of 0.1. This shows that the scatter in the fatigue behavior is significantly smaller at the higher stress as expected.

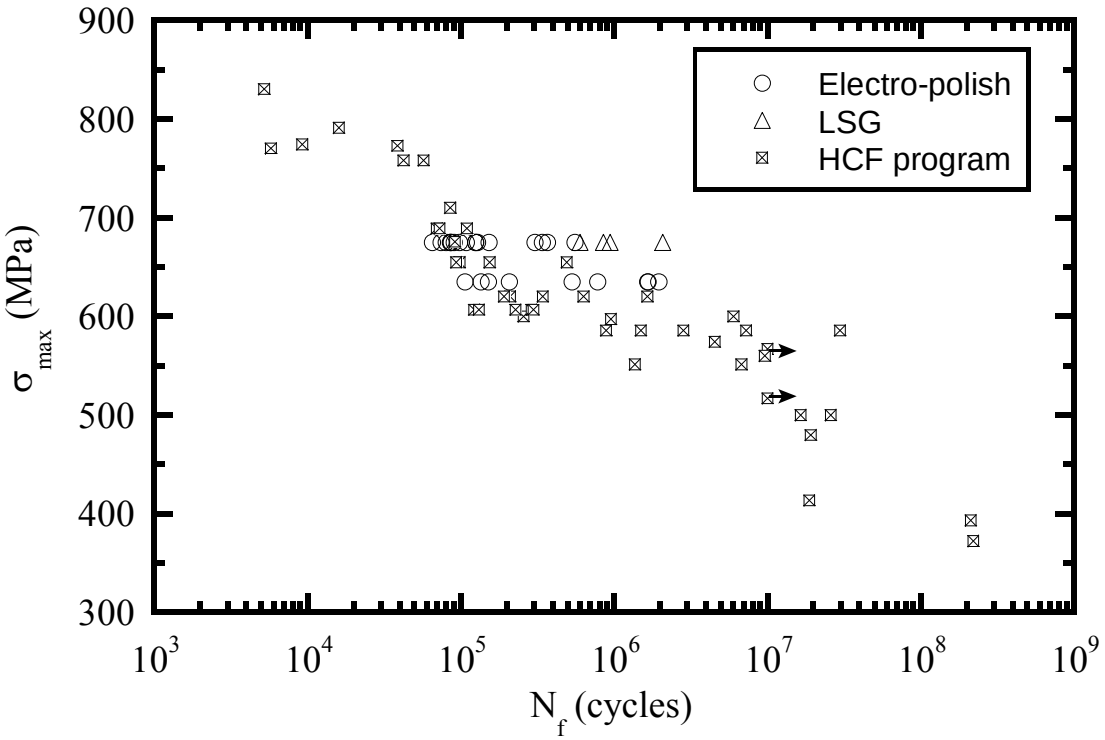

Figure 4: Stress-life plot of all data in this study along with data from the HCF program [10].

Testing of the LSG surface condition resulted in significantly longer lives at 675 MPa when compared to both the electropolished data and the HCF program data. All 5 specimens had longer lives than any of the electropolished samples. This could be attributed to the compressive residual stress on the specimen surface due to the LSG machining. Despite the compressive residual stresses at the surface, all of the LSG specimens nucleated cracks on the surface.

The same data from Fig. 4 was also plotted on the lognormal probability plot in Fig. 5. Here, the x-axis is the life in cycles on a log scale and the y-axis is the cumulative probability of failure. The LSG and electropolished specimen data, but not the HCF program data were plotted. The filled symbols are the electropolished (E-p) data and the open symbols are the LSG data. The electropolished data at both 675 MPa and 635 MPa have a larger than typical data set. The scatter in the data is especially visible on a probability plot and the electropolished data at

675 MPa spans slightly more than an order of magnitude. The distribution of data appears to be bimodal as has been observed in many other materials. These two modes in the failure distribution can be referred to as short life and long life, however, the underlying physical modes of failure causing this difference in behavior have not been identified. The distribution of data at 635 MPa has an even broader scatter than at 675 MPa despite having less data. Two few data currently exist to identify two distinct modes of behavior at 635 MPa. Likewise for the LSG data, there is too few data to identify modes of behavior. What is very clear is that the LSG data has a significantly longer mean life than the electropolished data as was observed on the S-N diagram. The mean of $\log_{10}(N_f)$ is approximately 145,000 cycles and 1,000,000 cycles for the electropolished and LSG surface treated specimens, respectively.

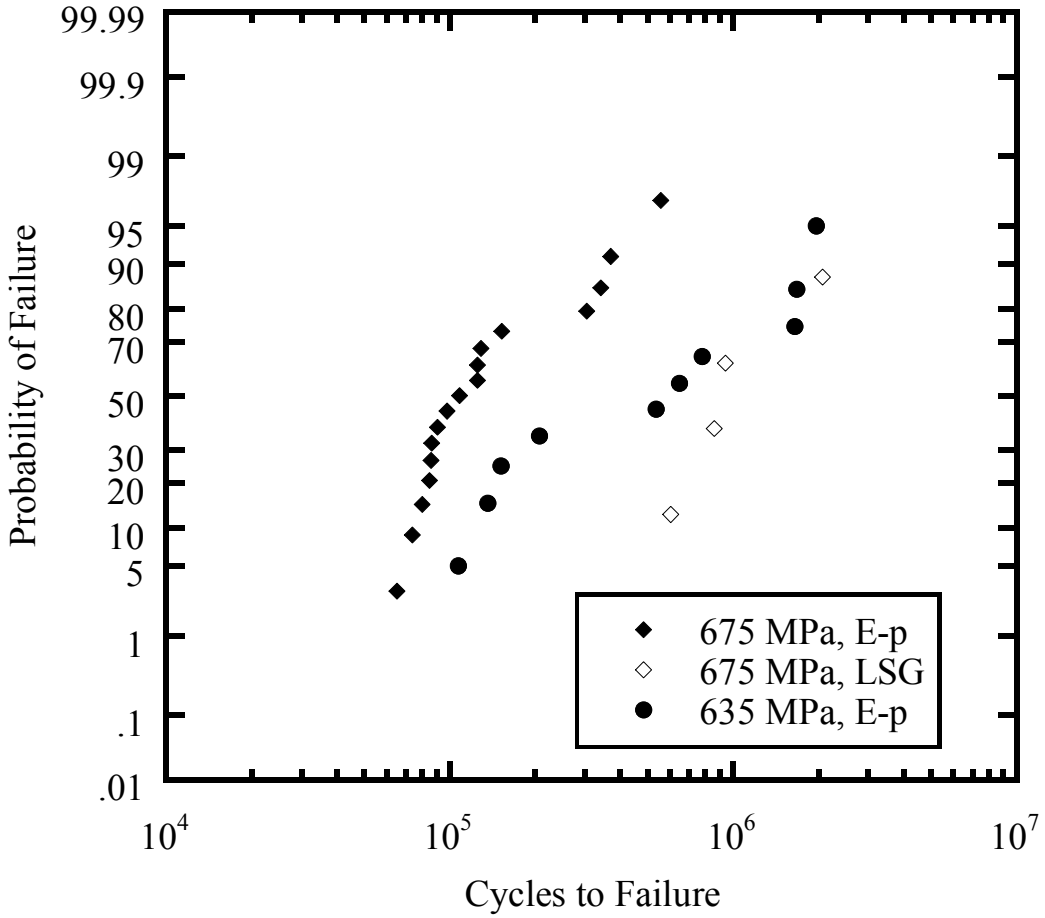

Figure 5: Probability plot of failures at all stresses and surface conditions at R = 0.1. The arrows indicate runout tests.

In addition to generating data for the S-N diagrams, several of the tests were also stopped intermittently for surface replication as described in the Experimental Procedures section. Example photographs from two replicas of the same specimen tested at 675 MPa and R = 0.1 at 45,000 cycles and 70,000 cycles are shown in Fig. 6. The total surface crack measurement is referred to as length 2*c* and 9 measurements of crack lengths were taken for this specimen. Surface crack length, *c*, is plotted versus cycles, *N*, in Fig. 7. The last crack size for this

specimen was measured at 80,000 cycles just prior to failure at 80,046 cycles. The crack begins at a size 2*c* of approximately 68 μm which is equivalent to 4 grains across. Once growth begins, the growth rate increases rapidly with crack size as expected and the crack growth life from the smallest identified crack is approximately 40,000 cycles for this specimen. A total of 7 electropolished fatigue tests have had replicas taken including 6 at 675 MPa and 1 at 635 MPa. The number of crack measurements per test ranged from 1 to 9, but 4 was the most common. The measured crack growth lives at 675 MPa ranged from 25,000 cycles to 40,000 cycles with initial measured crack sizes between 33 μm and 47 μm. A more useful way to evaluate this crack growth data is on a d*c*/d*N* versus Δ*K* plot, where d*c*/d*N* is the rate of surface crack growth and Δ*K* is the stress intensity factor range at the surface breaking point of the crack.

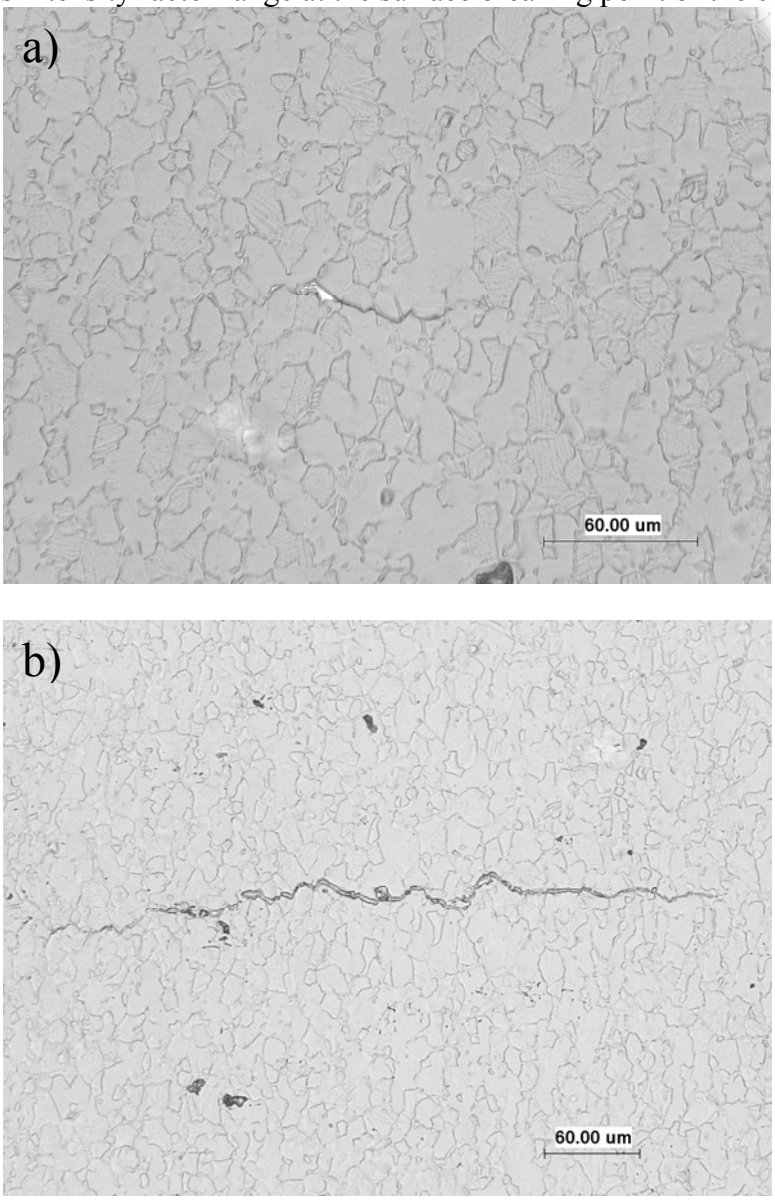

Figure 6: Example micrographs from specimen replicas showing the crack at a) 45,000 cycles and b) 70,000 cycles.

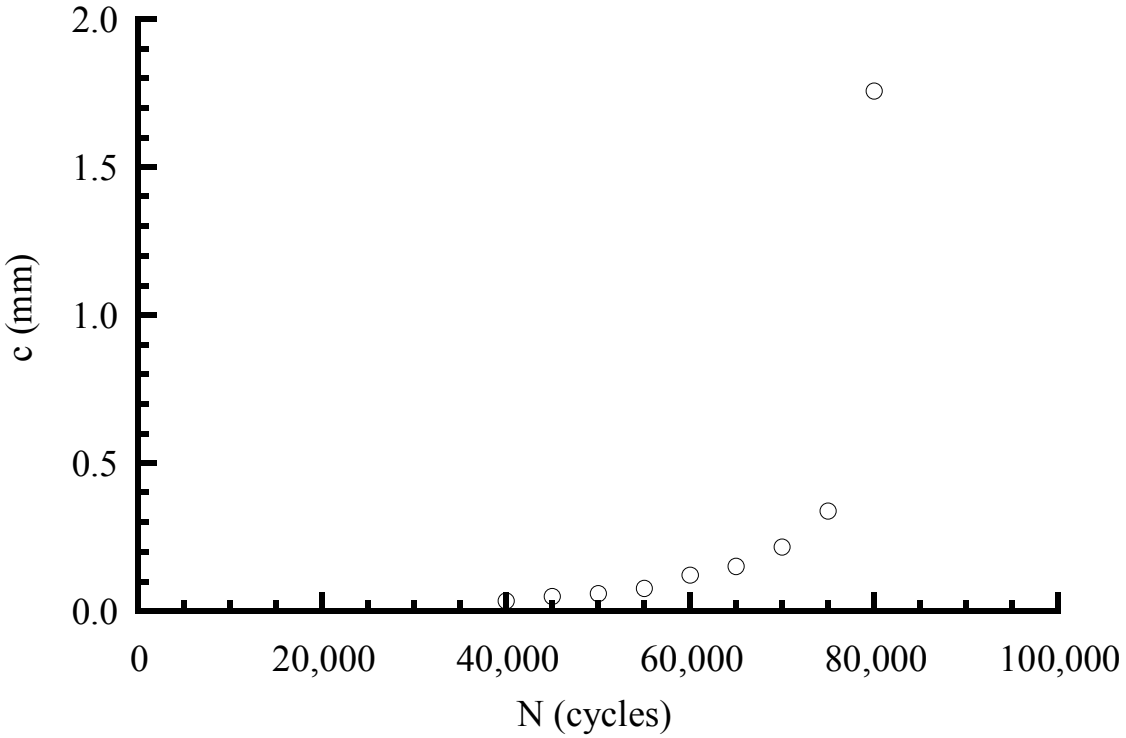

Figure 7: Plot of surface crack length versus cycles data measured from replicas.

Naturally initiated crack growth data, d*c*/d*N* versus Δ*K*, are plotted on Fig. 8 and are indicated by triangles. The growth data were reduced from the *c* versus *N* curves using the methods described in the previous section for 5 specimens tested at 675 MPa and R = 0.1. The other 2 specimens tested with replicas did not have enough crack measurements to produce d*c*/d*N* data. Several sets of previously published data are also plotted in Fig. 8 all from the same Ti-6Al-4V material used in the HCF program. These include long crack data tested at two frequencies by Boyce and Ritchie [15], small crack data from the HCF program [10], and small crack data from [16]. Here we will define small cracks as small with respect to the microstructure (grain size) in both the depth and surface length. Short cracks are defined as larger than small cracks and sampling many grains on the surface, but physically short relative to linear elastic fracture mechanics assumptions and other influences such as closure. Also plotted in Fig. 8 is a simple power law fit that follows the long crack data at high values of Δ*K* and captures the mean behavior of the small crack data from [10,16] at low values of Δ*K*. The data from the current study seems to fall along the transition regions from small crack to short crack and long crack data. Although the smallest crack sizes measured were near the definition of microstructurally small, the minimum applied Δ*K* (5. 6 MPa$\sqrt{\text{m}}$) is well above the observed long crack Δ*K* threshold, therefore, no significant increases in d*c*/d*N* over the long crack data were observed. This data tends to follow the *R* = 0.1 small crack fit line which deviates from the long crack data below Δ*K* values of 10 MPa$\sqrt{\text{m}}$.

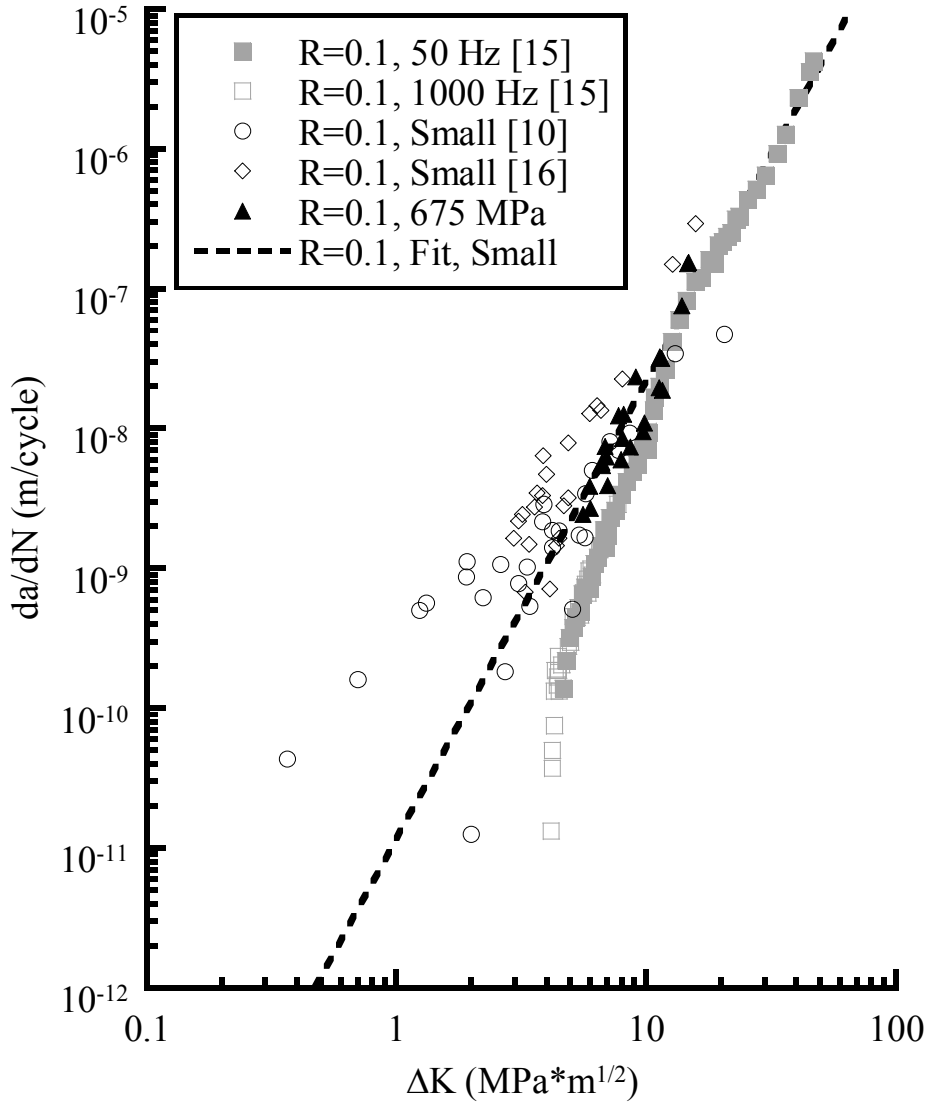

Figure 8: Fatigue crack growth rate data from this study and prior work.

Fractography has been conducted to identify the location and nature of the crack nucleation. Fig. 9 is an example of fractographs from an electropolished specimen with a surface crack initiation. River-marks can be seen in Fig. 9a that identify the source of the crack nucleation on the surface of the specimen. The higher magnification image in Fig. 9b shows the origin of the dominant crack that caused failure. The flat facet identified by the arrow is an alpha grain which is a typical crack initiation site in Ti-6Al-4V. All fractographs on both the electropolished and LSG samples have shown only surface initiated cracks that all appear to start at alpha grains. The initiation sites for the two surface conditions are indistinguishable. It was hypothesized that the compressive residual stress gradient at the surface of the LSG specimens might result in some specimens with subsurface crack initiation sites, but that has not yet been observed. Typical sizes of the alpha grain initiation sites range from 5 to 15 μm into the depth of the material.

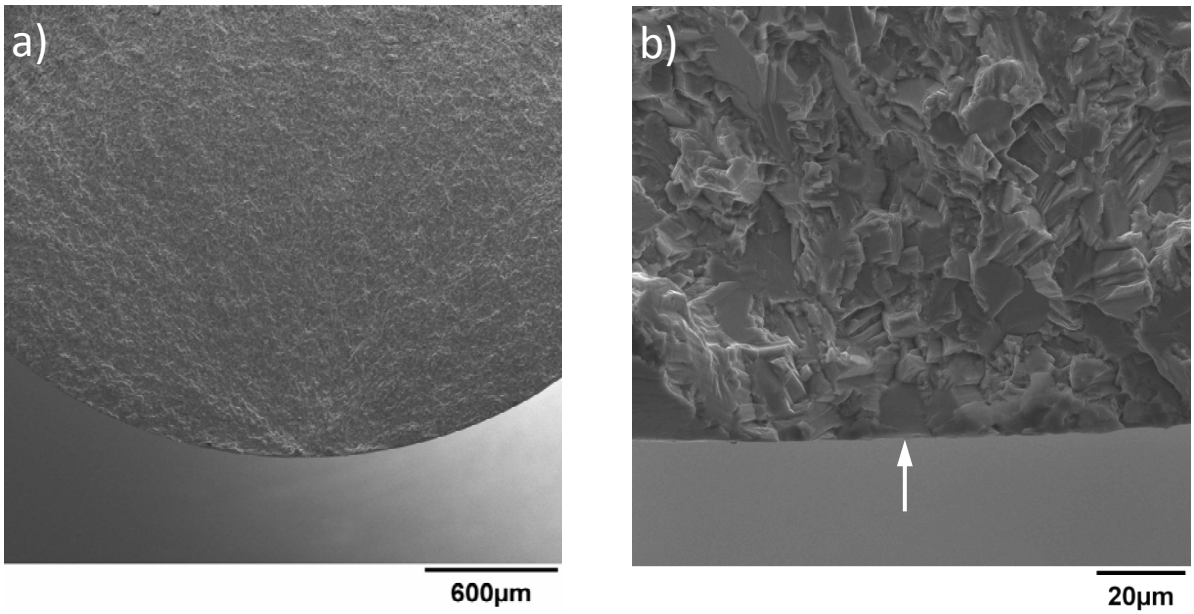

Figure 9: Example fractographs of an electropolished specimen with a surface crack initiation showing a) the fatigue crack growth topology and b) the location of the alpha grain initiation site.

A deterministic fracture mechanics life prediction was performed using the small crack growth data fit described above. The crack shape was assumed to remain $a/c = 1$ throughout the crack growth life. The initial crack for the analysis was assumed to be an alpha grain initiation at the surface of the specimen. Typical sizes of alpha grain facets from fractography were used. No residual stress was included in the fracture mechanics calculations, so only the SRA and electropolished tests were modeled. Fig. 10 is an S-N plot of the electropolished specimen data along with crack growth predictions for stresses between 575 MPa and 725 MPa with $R = 0.1$, and for initial crack sizes of 5, 10, and 15 µm. The analysis shows that the lives of the low life specimens can be primarily attributed to crack growth from an alpha grain with very little crack nucleation time. This is true at both 675 MPa and 635 MPa, however, the higher stress tends to have a higher proportion low life specimens than at the lower stress. This is very consistent with what has been observed in other materials [8-9]. With higher stress the failures become more dominated by crack growth, and the scatter in $\log_{10}(N_f)$ is smaller.

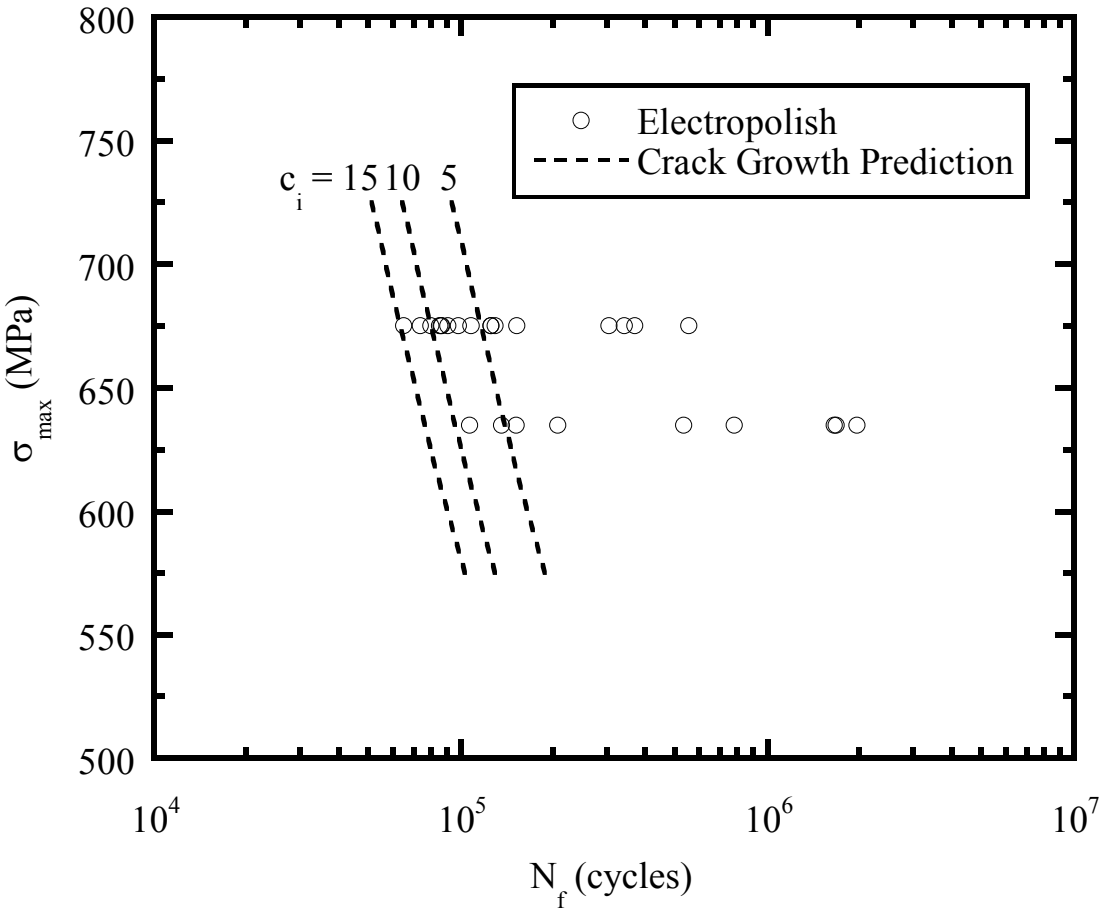

Figure 10: Specimen fracture mechanics life predictions using short crack growth lives with the initial crack size shown.

As this work and other researchers have shown, two modes of behavior often become apparent when significant numbers of specimens are tested under the same loading conditions. One mode is low failure life specimens which are crack growth dominant. The other mode is long lives which are crack nucleation dominant. As discussed earlier, this has been observed in many aerospace materials and can often be linked to distinct crack nucleation mechanisms. In the case of Ti-6Al-4V, cracks do not nucleate from material anomalies such as particles or pores so a physical mechanism that could explain two or more modes of behavior has not been identified. A possible explanation for the low life failure mechanism that is being investigated includes a favorable orientation of grains surrounding the initiating alpha grain. A lack of known mechanisms that controls the modes of behavior, however, should not stop the analyst from using this information when modeling the material behavior. It is important to consider bimodal or multimodal material behavior in the design of a component, particularly if the design criterion is the probability of failure. There is great potential to model the low probability tail of the component failure distribution incorrectly if an incorrect assumption about the material fatigue failure distribution is used.

5. Conclusions

Several conclusions can be made from the results of this study. It is shown that significant numbers of repeat fatigue tests at a single loading condition can result in distributions of fatigue lives that are not normal or lognormal. Instead, they often appear to be bimodal distributions which would likely never be observed under a typical materials test program due to too few tests at a given loading condition. This shows that the lower tail of the material fatigue failure distributions that are typically used for design of fatigue critical aerospace components may be incorrectly predicted without adequate data to model the distribution. Crack initiation sites in this alpha+beta processed Ti-6Al-4V were exclusively surface located alpha grains. The low life mode of the bimodal distributions was shown to be effectively modeled by crack growth with no nucleation time using small crack growth data. This may be an effective approach for estimating the limiting fatigue behavior of Ti-6Al-4Vwith greater confidence without testing large numbers of specimens at each load condition.

Acknowledgements

This work was performed at the Air Force Research Laboratory, AFRL/RXLMN, Materials and Manufacturing Directorate, Wright-Patterson Air Force Base, and was partially supported under AF Contract No. FA8650-04-C-5200.

References

[1] U.S. Air Force, Engine Structural Integrity Program, Military Standard 1783B, Aeronautical Systems Center, Wright-Patterson Air Force Base, OH, 31 May 2002.

[2] U.S. Air Force, Aircraft Structural Integrity Program, Military Standard MIL-STD-1530C(USAF), Wright-Patterson Air Force, OH, 1 Nov. 2005.

[3] Materials Damage Prognosis, J.M. Larsen, L. Christodoulou, J.R. Calcaterra, M.L. Dent, M.M. Derriso, W.J. Hardman, J.W. Jones, and S.M. Russ, Eds., TMS, Warrendale, PA, 2005.

[4] Magnusen, P.E., Bucci, R.J., Hinkle, A.J., Brockenbrough, J.R., and Konish, H.J., "Analysis and Prediction of Microstructural Effects on Long-Term Fatigue Performance of an Aluminum Aerospace Alloy," International Journal of Fatigue, Vol. 19, Supp. No. 1, pp. S275–S283, 1997.

[5] Chan, K.S. and Enright, M.P., "A Probabilistic Micromechanical Code for Predicting Fatigue Life Variability: Model Development and Application," Journal of Engineering for Gas Turbines and Power, ASME, Vol. 128, pp. 889-895, October 2006.

[6] Tryon, R., Dey, A., and Krishnan, G., "Microstructural-Based Physics of Failure Models to Predict Fatigue Reliability," Journal of the IEST, V. 50, No. 2, pp. 73-84, 2007.

[7] Laz, P.J., Craig, B.A., and Hillberry, B.M., "A probabilistic Total Fatigue Life Model Incorporating Material Inhomogeneities, Stress Level and Fracture Mechanics," International Journal of Fatigue, Vol. 23, S119–S127, 2001.

[8] Jha, S.K., Larsen, J.M., Rosenberger, A.H., and Hartman, G.A., "Dual Fatigue Failure Modes in Ti-6Al-2Sn-4Zr-6Mo and Consequences on Life Prediction," Scripta Materialia, Vol. 48, pp. 1637-1642, 2003.

[9] Jha, S.K., Caton, M.J., and Larsen, J.M., "A New Paradigm of Fatigue Variability Behavior and Implications for Life Prediction," Materials Science and Engineering A, Vol. A468-470, pp. 23-32, 2007.

[10] "Improved High Cycle Fatigue (HCF) Life Prediction", Eds. Gallagher, J.P, et al., AFRL-ML-WP-TR-2001-4159, Wright-Patterson AFB, OH 45433.

[11] Standard test method for measurement of fatigue crack growth rates. ASTM E647-00, Annual Book of ASTM Standards. American Society for Testing and Materials; 2002.
[12] Forman, R.G., Shivakumar, V., "Growth Behavior of Surface Cracks in the Circumferential Plane of Solid and Hollow Cylinders," Fracture Mechanics: Seventeenth Volume, ASTM STP 905, J.H. Underwood, R. Chait, C.W. Smith, D.P. Wilhem, W.A. Andrews, and J.C. Newman, Eds., American Society for Testing and Materials, 1986, pp. 59-74.
[13] Raju, I.S., Newman, J.C., "Stress-Intensity Factors for Circumferential Surface Cracks in Pipes and Rods under Tension and Bending Loads," Fracture Mechanics: Seventeenth Volume, ASTM STP 905, J.H. Underwood, R. Chait, C.W. Smith, D.P. Wilhem, W.A. Andrews, and J.C. Newman, Eds., American Society for Testing and Materials, 1986, pp. 789-805.
[14] Moore, M.G., Evans, W.P., "Mathematical Correction for Stress in Removed Layers in X-Ray Diffraction Residual Stress Analysis," SAE Transactions, Vol. 66, 1958, pp. 340-345.
[15] Boyce, B.L., Ritchie, R.O., "Effect of Load Ratio and Maximum Stress Intensity on the Fatigue Threshold in Ti-6Al-4V," Engineering Fracture Mechanics, Vol. 68, 2001, pp. 129-147.
[16] Peters, J.O., Roder, O., Boyce, B.L., Thompson, A.W., Ritchie, R.O., "Role of Foreign Object Damage on Thresholds for High-Cycle Fatigue in Ti-6Al-4V," Metallurgical and Materials Transactions A, 31A(6), 2000, pp. 1571-1583.